Large elongations in WE54 magnesium alloy by solute-drag creep controlling the deformation behavior

O.A. Ruano, M. Álvarez-Leal, A. Orozco-Caballero[+], F. Carreño
Physical Metallurgy Department, CENIM-CSIC, Av. Gregorio del Amo 8, 28040 Madrid, Spain
([+]) Now at: Department of Mechanical Engineering, Chemistry and Industrial Design, Polytechnic University of Madrid, Ronda de Valencia 3, 28012, Madrid, Spain.

Abstract

Solute-drag creep is a diffusion-controlled process that may govern deformation in coarse-grained materials with solute atoms in solution. Elongation-to-failure tensile tests were conducted in a WE54 alloy containing solutes of Y and Nd in the range 25 to 450 ºC. Elongations of more than 150% were observed at high temperatures and a maximum elongation to failure of 312% was determined at 450 ºC and 10^{-2} s^{-1}. Microstructural observations show elongated grains and the presence of dislocation bands after deformation under these conditions. Strain-rate-change tests reveal a range at high temperatures showing low stress exponents. Since grain boundary sliding was discarded as a possible controlling mechanism, the observed low stress exponents, high elongations and elongated grains are attributed to solute-drag creep as the principal deformation mechanism.

Keywords: Magnesium WE54; Ductility; High Temperature Deformation Mechanisms; Solute Drag Creep

1. Introduction

Magnesium WE54 alloy is a heat treatable high strength casting alloy. It combines high strength–density ratio with excellent mechanical properties and it can be used in structural applications at temperatures up to 300°C [1]. Additionally, the presence of yttrium provides good corrosion resistance to this alloy. However, this alloy has very limited formability during conventional forging processes at elevated temperature.

It is well known that Y, Nd and RE are elements that significantly strengthen the magnesium-based alloys due to their large atomic size and large solubility [1–4]. The alloy elements are usually combined during the melting process prior to cast in the form of magnesium base master alloys [4,5]. This process is normally carried out using electric furnaces in the presence of an oxygen and humidity free atmosphere. Such alloy strengthening is caused by precipitation hardening and solid solution hardening [2,6–10]. At the same time, these elements improve the ductility by weakening the recrystallization texture [11–13]. Additionally, it is worth to mention that the activation energies for the diffusion of these elements in the magnesium matrix are high and the diffusivity values are low and, therefore, the precipitation kinetics is strongly influenced by temperature [9].

It has been demonstrated in the last decades that the mechanism of grain boundary sliding (GBS) allows reaching very high elongations to failure [14–16]. This has an important application in the manufacturing industry to form complex parts from metallic sheets. However, there is another deformation mechanism that has been observed to reach large elongations in Al-Mg alloys [17,18]. This mechanism is solute drag creep or viscous-glide creep, which depends on the solute atoms that are present in solid solution in some materials. Usually, a high size difference between the matrix and the solute atom favors the drag effect. Therefore, not all solutions in materials may impede dislocation motion by solute drag but Al and Mg are two metals that have been shown to exhibit solute drag creep [19–21]. As it will be shown, the WE54 contains elements in solid solution especially at high temperature or after controlled thermal treatments that are candidates to interact with gliding dislocations.

Solute drag creep is a dislocation creep mechanism that is in competition with climb controlled dislocation creep since it is known that creep occurs by a sequential process involving glide and climb processes. Both should elongate the grains after deformation. The slower of these processes is controlling deformation. Usually climb is the slower of the processes but in the case of dislocations hindering their movement, for instance, by the presence of solute atoms, glide would be the rate controlling process.

Weertman [22] developed a theory for creep based on the dislocation motion controlled by the velocity of solute drag where the strain rate is the following power-law equation:

$$\dot{\varepsilon} = A D_{sol} (\sigma / E)^3 \quad (1)$$

where the stress exponent, n, is three, A is a constant and D_{sol} is the diffusion of the particular controlling solute in the matrix.

Finally, in the same range of temperatures and strain rates where GBS and solute-drag take place, a third mechanism, conventional slip creep (n ~ 5), may also be active. However, this mechanism shows lower strain rate sensitivity, m (being m the inverse of the stress exponent, n), and usually leads to smaller elongations to failure [22,23].

In the current context for producing metallic materials with large ductility values, useful for any forming processes, it is key to avoid as much as possible any prior thermomechanical treatments, minimizing the total cost. In the present research, we elucidate the active creep mechanisms responsible of the large ductility observed in this alloy and the underlying reasons for the observed mechanical behavior from room to high temperatures.

2. Material and experimental procedure

The chemical composition of the WE54 magnesium alloy used in the present investigation has the following approximate nominal composition in weight %: 5-5.5% Y - 1.5-2% Nd - 1.5-2% RE - 0.45% Zr, balance Mg.

The material was received in the form of extruded plates 300 x 80 x 5 mm^3 in the T6 condition. In this kind of magnesium alloys this temper is usually reached by solution-treating at 525 ºC for 8 h, followed by quenching into hot water (60 ºC) and a final aging at 250 ºC for 12 h [24]. Samples were heat treated at different temperatures, intervals and cooling rates with the purpose of reaching minimum hardness. This minimum hardness condition was denominated TT condition.

Samples for electron backscatter diffraction (EBSD) were prepared by standard preparation including mechanical polishing and chemical polishing for 5-10 s using a solution comprising 4.2 g picric acid, 10 ml acetic acid, 10 ml H_2O and 70 ml ethanol. A 2% Nital etchant was used for optical microscopy studies.

Tensile samples of 6 mm gage length were machined out of the plate with their longitudinal axis parallel to the extrusion direction. The tensile tests in the T6 and TT

condition were carried out at 10^{-2} s^{-1} and at temperatures in the range 20 to 450 ºC. Vickers hardness tests were conducted with a diamond indenter under 10 N load.

Strain rate change tensile tests were conducted at temperatures in the range 300 to 450 ºC. These tests were initiated by deforming the samples 15% at 10^{-2} s^{-1} and then decreasing the strain rate in several steps down to 10^{-5} s^{-1}. In each step, the sample was deformed about 3%.

3. Results and discussion

3.1. Hardness tests

The as-received WE54 alloy, in the T6 temper condition, showed HV = 89, which was taken as the maximum hardness value in this alloy. Various heat treatments were selected to reach the minimum hardness in order to compare microstructures and determine its influence in the mechanical properties at high temperature.

Fig. 1 shows the hardness values as a function of time. Minimum hardness values of 78 and 73 HV are obtained after 2 and 1 h at 200 and 280 ºC, respectively. For longer treatment times, the hardness increase progressively up to values of 85 and 80 HV for 200 and 280 ºC respectively. Taking into account this evolution, additional tests were conducted at higher temperatures, 450 and 520 ºC, and cooling rates of 8 ºC/min reaching values of 72 and 69 HV respectively. These last two tests showed the importance of the cooling rate on the mechanical properties. Therefore, a lower cooling rate of 1 ºC/min was selected to obtain the lowest hardness value of 62 HV from 500 ºC, named TT condition.

3.2. Microstructure

The microstructure of the as-received material (named T6 condition) is given in Fig. 2. The figure shows equiaxed grains varying between 50 and 250 μm. An average grain size of 150 μm was determined by means of the linear intercept method.

The morphology of the grains and precipitates of the temper with the highest hardness values, T6 condition, and its evolution with the heat treatment was studied through SEM micrographs. Fig. 3 gives details of two regions of the microstructure corresponding to Fig. 2.

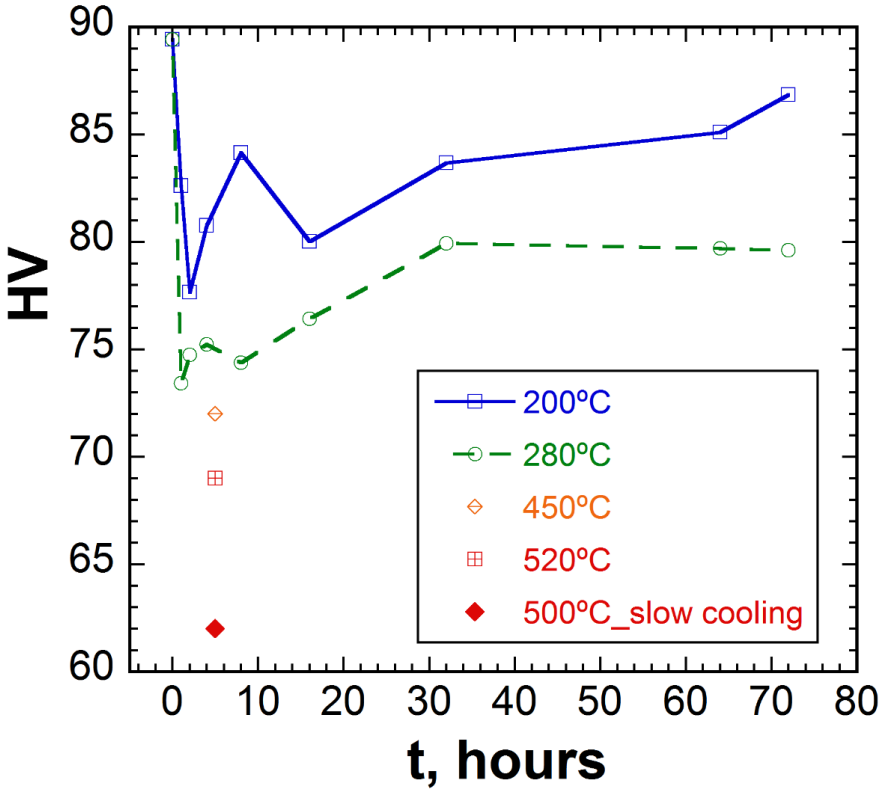

Fig. 1. Hardness as a function of annealing time for the WE54 alloy. Cooling rates in the samples at high temperature corresponded to furnace cooling.

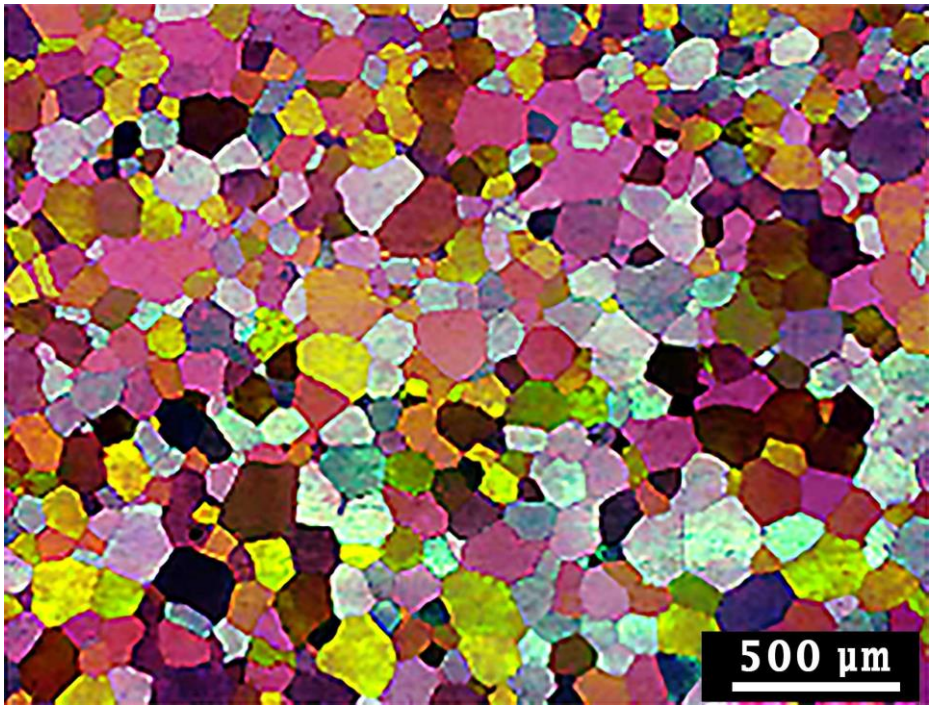

Fig. 2. Optical micrograph of the as-received WE54 material, named T6 condition.

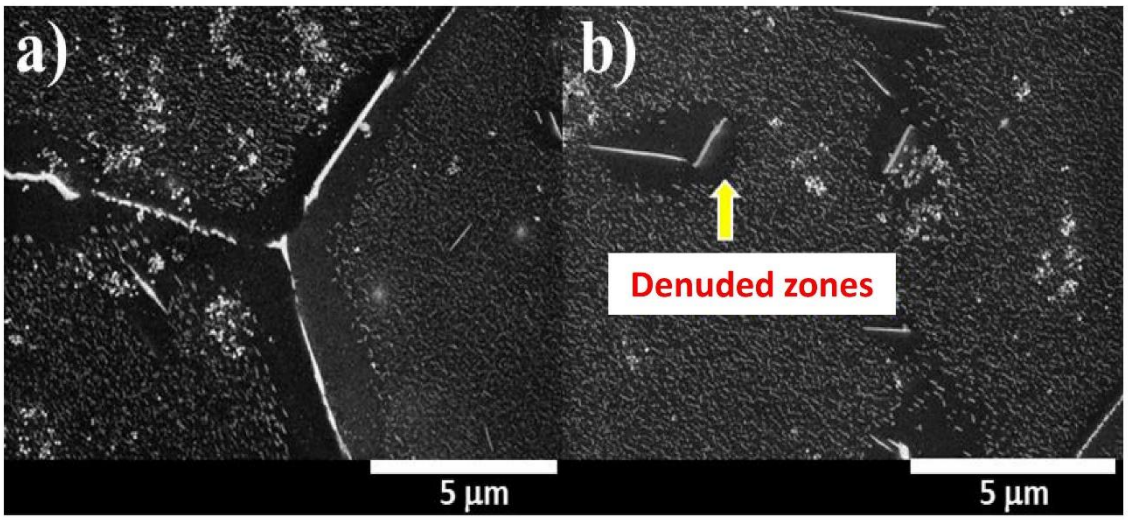

Fig. 3. SEM micrographs of the WE54 magnesium alloy in the T6 condition showing a) the disposition of precipitates and denuded zones at grain boundaries and b) denuded zones around lenticular precipitates of large size.

The volume fraction of the precipitates was 11.5%. Fig. 3 shows a high amount of precipitates of lenticular morphology and different sizes. The smaller and more abundant are about 100 nm large and 10 nm width and are situated in the interior of the grains, Fig. 3(b), distributed following a prismatic-planes habit. It is our contention that these precipitates can be identified as β_1 (Mg_3Nd) similarly to the ones found elsewhere, [10,24]. The larger particles are about 2-4 µm long and 50 nm wide. These precipitates are surrounded by a denuded zone as shown in Fig. 3(b). Another group of precipitates, far much scarcer and distant, is that with a square prismatic structure of 1 to 4 µm in size. Finally, there are large precipitates of about 50 to 100 nm in thickness decorating the grain boundaries. The diffusion of solutes towards these boundaries left behind denuded zones that are around 3 µm in width.

Fig. 4 shows micrographs of WE54 T6 after thermal treatments, corresponding to 200 and 280 ºC during 2 and 72 h followed by fast cooling. The micrographs that correspond to the low hardness values of Fig. 1 at 200 and 280 ºC are given in Fig. 4(a) and (c), respectively. It should be noted that the minimum hardness was reached for treatments of 1 h at 280 ºC but the microstructures are similar to those of 2 h presented in the figure.

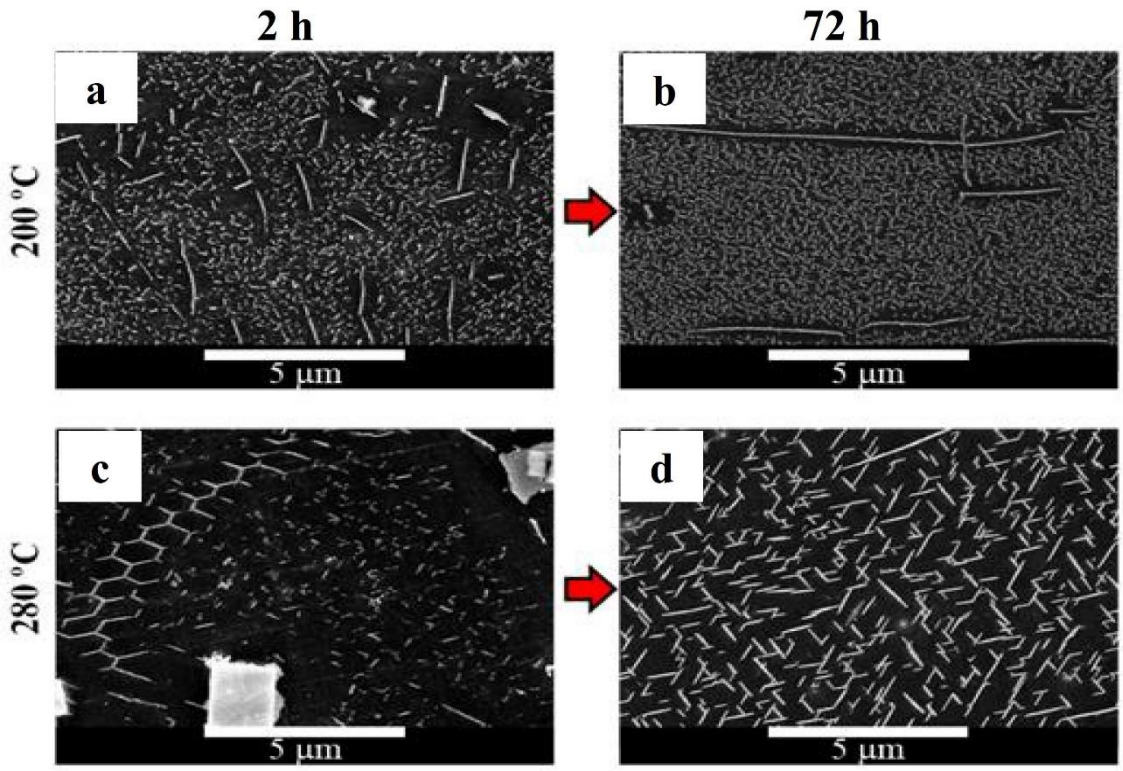

Fig.4. SEM micrographs for WE54 T6 samples treated at 200 and 280 ºC at 2 and 72 h followed by fast cooling: a) 200 ºC/2h, b) 200 ºC/72h, c) 280 ºC/2h, and d) 280 ºC/72h.

After two hours at both temperatures, 200 and 280 ºC, the volume fraction of precipitates increases. At 200 ºC the precipitates have the same morphology than those of Fig. 3 in the T6 condition. In contrast, at 280 ºC for 2 h, Fig. 4c, a higher amount of large lenticular precipitates is formed, in many cases in a hexagonal lay-out.

Large hardness values are observed after 72 h at 200 ºC, and moderate hardness at 280 ºC (Fig. 1). The corresponding microstructures are shown in Fig. 4b and d, respectively. At 200 ºC, new and very small, finely distributed lenticular particles cover the entire magnesium matrix. At the same time, some large lenticular particles grow notably along their longitudinal axes. In contrast, at 280 ºC/72 h, large precipitates are located in the interior of the grains forming angles of about 120º.

Fig. 5 shows micrographs of the samples annealed at 480 and 520 ºC for 5h and furnace cooling, i.e. at low cooling rates of about 8 ºC/min, corresponding to low hardness values in Fig. 1. The microstructure at 500ºC was almost the same as that at

520ºC and is not included in the figure. In both cases, the microstructures are similar and consist of a lower amount of precipitates in the matrix and a higher concentration at grain boundaries. Both conditions present lenticular and prismatic precipitates. Their size and separation are larger than those observed in Fig. 4 at lower annealing temperatures, which explains the low hardness observed. It is concluded that a minimum hardness is observed for annealing at a high temperature to obtain large precipitates, distant from each other, and cooled down at a very low cooling rate to allow the solute atoms to migrate toward the precipitates. In this way, moreover, a low amount of solutes remains in solid solution diminishing its hardening effect.

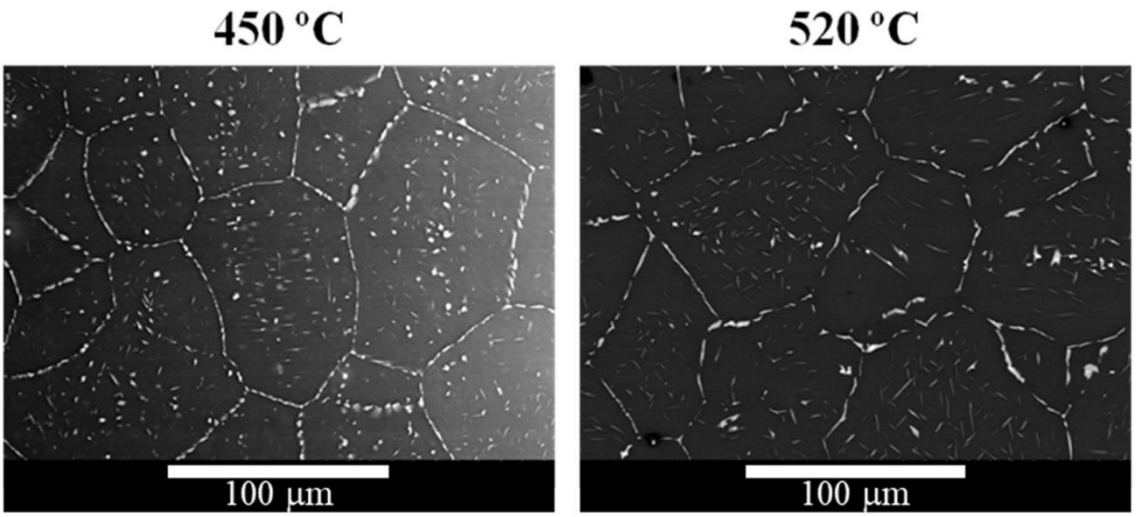

Fig. 5. SEM micrographs of thermal treatments for 5 h and slow cooling in furnace from a) 450 ºC and b) 520 ºC.

3.3. Tensile tests to fracture

Stress-strain curves at an initial strain rate of 10^{-2} s^{-1} tested from room temperature to 450 ºC for the WE54 magnesium alloy in the thermal treatment conditions T6 and TT are given in Fig. 6.

Table 1 shows the values of the mechanical parameters extracted from Fig. 6: yield stress ($\sigma_{0,2}$), ultimate tensile stress (UTS), uniform strain (e_u) and elongation to failure (e_f).

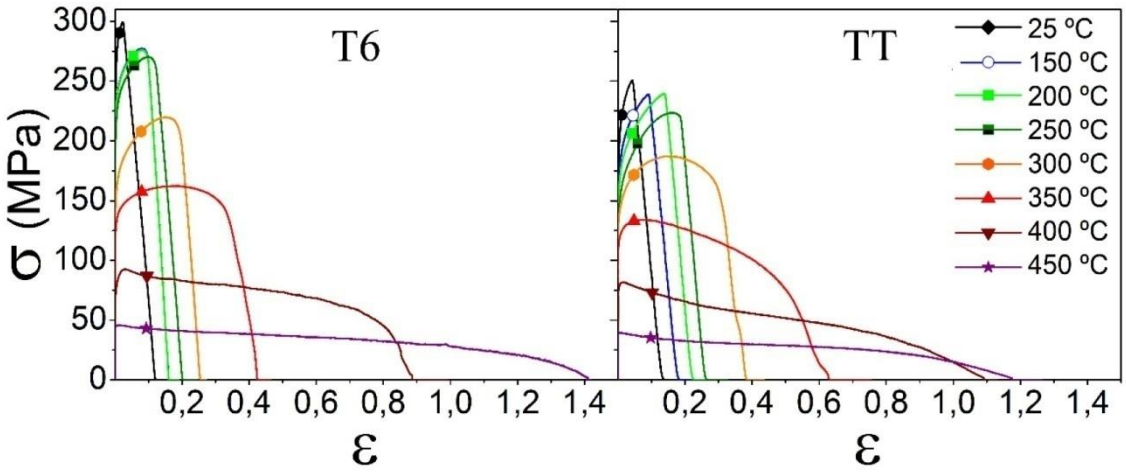

Fig.6. Stress-strain curves at 10^{-2} s^{-1} and various temperatures for the WE54 magnesium alloy in the thermal treatment conditions T6 and TT.

Fig. 7 shows the variation of the UTS with temperature for the T6 and TT conditions. The higher values of the stress for the T6 condition is attributed to the higher concentration of solute atoms in the matrix and the smaller size of precipitates. Above 250 ºC there is an increasing dissolution of precipitates and increasing amount of solutes with temperature, so that the mechanical behavior of both conditions tend to converge.

The elongation to failure as a function of temperature extracted from the constant strain rate tests at 10^{-2} s^{-1} in both states is shown in Fig. 7. The ductility increases with temperature and a strong increase is observed above about 300 ºC with a maximum for the elongation to failure of 312% at 450 ºC in the T6 state. This is a remarkable result since the grain size is coarser than 150 μm at the start of the tests (Fig. 2). Furthermore, all microstructures after testing at high tempertature appear strongly elongated. As an example, Fig. 8 shows the microstructure of a sample in the T6 condition deformed 141%, at 400 ºC and 10^{-2} s^{-1}. Such coarse microstructure and the elongated appearance after testing eliminates grain boundary sliding as a possible dominant deformation mechanism, since this mechanism requires equiaxed grain sizes lower than 15 μm [14,25]. Additionally, the micrographs of Fig. 8 revealed dislocation bands within the

elongated grains after testing, which suggests that deformation is controlled by a slip creep mechanism.

Moreover, the very close values of UTS for both states at about 150-200 ºC, Fig. 7, and the slight ductility drop at 250 ºC for the T6 condition suggest the influence of solute effects, as it will be discussed later.

Table1. Mechanical parameters for the WE54 magnesium alloy for the T6 and TT conditions tested at 10^{-2} s^{-1} at various temperatures.

	T (ºC)	**$\sigma_{0,2}$ (MPa)**	**UTS (MPa)**	**e_u (%)**	**e_f (%)**
WE54 T6	25	245	299	2	3
	150	226	277	8	10
	200	252	276	8	17
	250	239	270	10	13
	300	147	220	16	22
	350	145	162	19	52
	400	74	92	2	141
	450	44	46	1	312
WE54 TT	25	181	251	4	14
	150	160	239	10	20
	200	152	239	15	25
	250	137	223	17	30
	300	132	187	18	46
	350	113	134	8	87
	400	75	82	2	197
	450	39	39	1	222

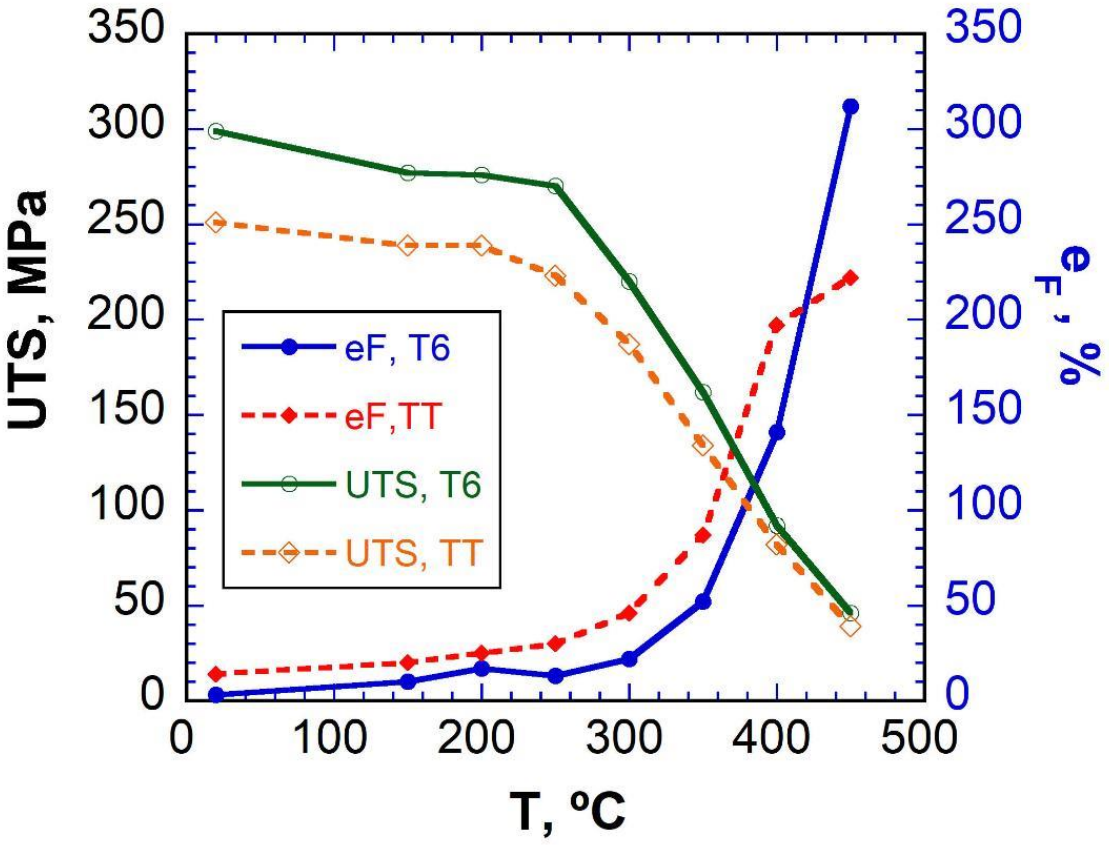

Fig. 7. The UTS and the elongation to failure as a function of temperature for the WE54 alloy tested at 10^{-2} s^{-1} in the T6 and TT conditions.

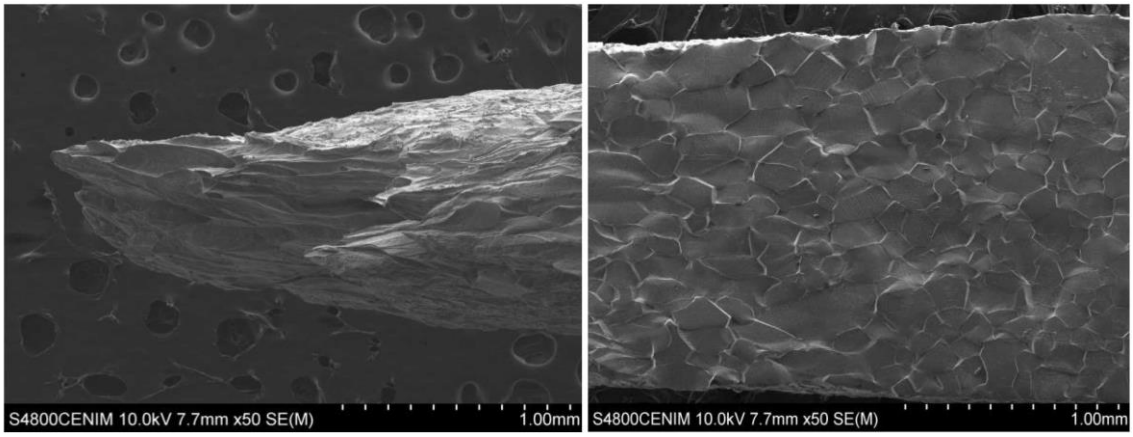

Fig. 8. Microstructure of a sample in the T6 condition deformed 141%, 400 ºC at 10^{-2} s^{-1}, a) low magnification and b) high magnification.

3.4. Strain rate change tensile tests

With the goal of assesing the deformation mechanism at various temperatures in the WE54 magnesium alloy in the T6 and TT conditions, a series of strain rate change tests were conducted to determine the stress exponents and the activation energies. Fig. 9 shows these tests at 300, 350, 400 and 450 ºC.

Two different stress exponent regions are observed in Fig. 9. At high strain rates, stress exponent values higher than 5 are observed corresponding to a slip creep mechanism. A transition to lower n values with decreasing strain rates is observed at all four temperatures. At low strain rates, values of n of about 3 are measured for the T6 and TT states at 350, 400 and 450 ºC. These values are close to the theoretical value of 3 for the solute-drag creep equation, Eq. (1). An estimation of the activation energy for deformation, at low strain rate, presented large scatter around values somewhat higher than Q_L, the activation energy associated to lattice self-diffusion. This fact is related with microstructure and mechanism changes, which vary from intermediate to high temperature as it will be explained below.

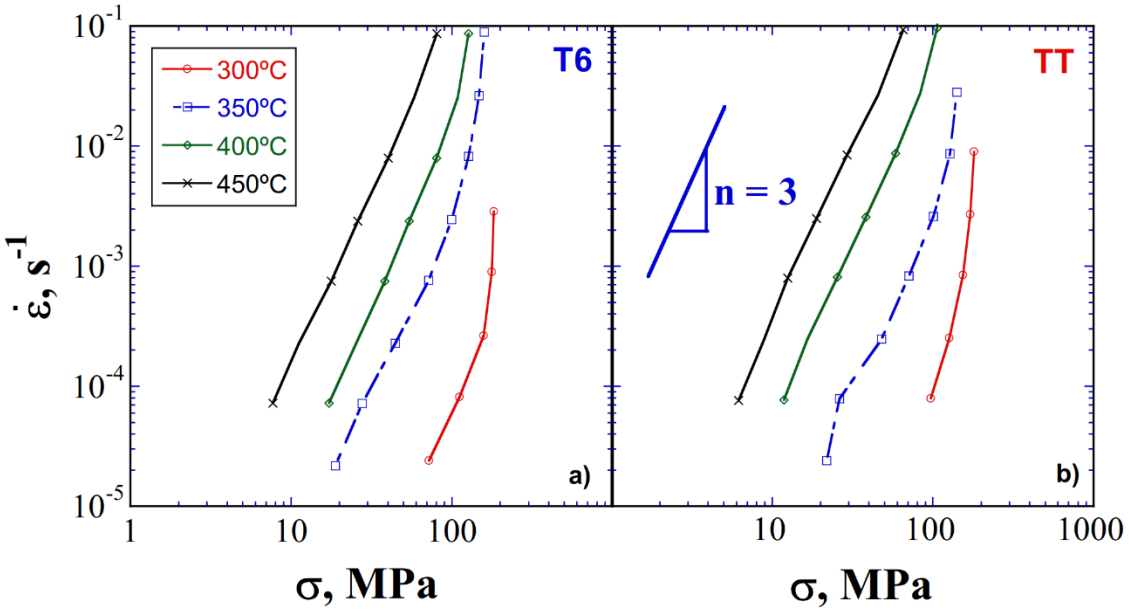

Fig. 9. Strain rate as a function of stress at temperatures in the range 300 to 450 ºC for WE54 alloy in the a) T6 condition, and b) TT condition.

3.5. *Deformation mechanisms*

The high temperature behaviour of the WE54 magnesium alloy differs from the conventional behaviour of most alloys since a progressive UTS decay is not observed as it is usually obtained in most alloys, Fig. 7. This behavior is schematically shown in Fig. 10 on hand of the results obtained previously. The data points correspond to those of Fig. 7. The figure shows on one hand, at high temperatures, a considerable drop of stress with increasing temperature which is typical of a solute drag mechanism with an associated n=3. On the other hand, for intermediate to low temperatures, a dynamic strain ageing (DSA) effect is present so that similar stress values can be obtained at a certain domain of strain rates and temperatures for which dislocations start moving faster than the dislocations containing solutes, also called solute clouds. This clouds are similar to the Cottrell atmospheres. For this strain rate and temperature domain the solute-drag mechanism is changing towards a conventional slip creep mechanism with higher stress exponents. For the WE54 alloy, this domain is around 150-250 ºC.

It is known that in the WE54 alloy system, Y and Nd are present as solutes. The atomic radius of these elements, including the heavy rare earth elements, as a measure of their size, is very different from the size of the Mg atom favoring the solute drag creep mechanism. Therefore, among the possible slip creep mechanisms, solute-drag creep is a solid candidate. This mechanism requires the presence of solutes that hinder the moving dislocations. As mentioned in the introduction, the constitutive equation for this mechanism is characterized at high temperatures by a stress exponent equal to 3, Eq. (1). According to several investigations [22,26–28], the elongation to failure is closely related to low stress exponents. A stress exponent of 3 can be considered to be a low value and this can explain the high elongations observed in this alloy. The peak in stress observed, for instance, at 400 ºC, Fig. 6, at the beginning of deformation, is also indicative of the presence of solutes. Furthermore, with increasing temperature increases the precipitates dissolution increasing the amount of solutes facilitating this mechanism.

A further proof of the operation of solute-drag creep is the behavior of the alloy at low temperatures. Fig. 7 shows almost no variation of the stress between room temperature and 250 ºC. This is valid for the T6 and for the TT conditions and is typical of the presence of solutes and the phenomenon of dynamic strain aging at relative low temperatures. Additionally, the remarkably low precipitate strengthening in magnesium

alloys is well known [29–31], while solute strengthening has a more important role for understanding the mechanical properties in magnesium alloys than in other alloy systems [32]. This relative low influence of precipitates occurs at both low and high temperatures. This behavior is similar to that found in an Al-Mg alloy, such that in this region the strength was reported to be independent of the temperature and also of the magnesium content [21,33]. It has been seen that this mechanism also operates in a WE43 magnesium alloy that contains similar alloying elements than the WE54 alloy but slightly less quantity of rare earth elements [27].

Additionally, another phenomenon could be contributing to the fast stress drop from intermediate temperatures and, especially, to the high ductility acceleration with increasing temperature for this magnesium based alloy. This phenomenon is related to the easier activation of the slip in the prismatic and pyramidal planes with increasing

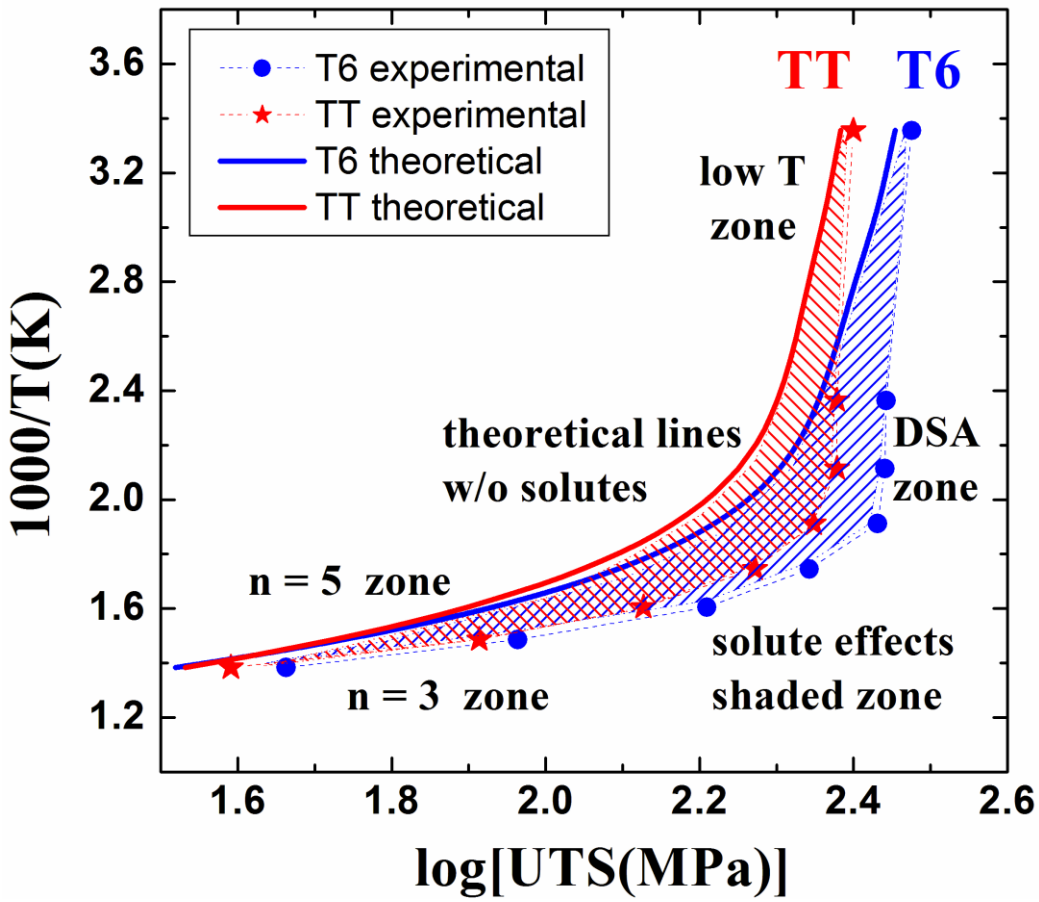

Fig. 10. Expected behavior (solid lines) without solute effects on both states of the WE54 magnesium alloy.

temperature, as their CRSS values get closer to that of the basal plane. Thus, there is an increasing number of slip planes available for deformation with increasing temperature [34].

In any case, the increasing number of slip planes should not change the underlying creep mechanism, associated to solute drag creep with n=3 at high temperature, but would increase dramatically the elongation to failure as deformation accommodation would be highly enhanced.

5. Conclusions

1. The microstructure of the as-received material shows equiaxed grains of sizes between 50 and 250 μm, containing lenticular precipitates of different sizes. The smaller and more abundant β_1 (Mg_3Nd) precipitates are about 100 nm large and 10 nm width and are situated in the interior of the grains, distributed following a prismatic-planes habit. The larger particles, about 2-4 μm long and 50 nm wide, are surrounded by a denuded zone.
2. Increasingly large elongations of more than 300% are obtained at increasing high testing temperature in a WE54 magnesium alloy having coarse grain sizes, higher than 150 μm in diameter. Grain boundary sliding is excluded as the mechanism governing deformation.
3. The large elongations to failure observed at high temperatures are related to the low value of the stress exponent, close to three. Such a low stress exponent raises deformation stability.
4. A solute-drag slip creep mechanism is proposed as the deformation controlling mechanism. The stress exponent close to three corresponds to that predicted by the constitutive equation of Weertman for this mechanism. The similar values of the stress found for each T6 and TT condition at high temperatures is in agreement with the influence of solid solution atoms.
5. A transition from n=3 at low stresses to larger n values at high stresses and lower temperatures (150–250ºC) is consistent with the end of the solute-drag mechanism giving rise to a domain of dynamic strain ageing (DSA) with low ductility values for both T6 and TT conditions. This DSA domain is also

consequence of the interaction between dislocations and solid-solution atoms present in the WE54 magnesium alloy.

Acknowledgements

Financial support from MINECO (Spain), Project MAT2015-68919-R (MINECO/FEDER) is gratefully acknowledged. A. O-C also thanks CENIM, CSIC, for a contract funded by the aforementioned project. M. A-L thanks MINECO for a FPI fellowship, number BES2013-063963 (MINECO/FEDER/ESF).

Data availability

The raw/processed data required to reproduce these findings cannot be shared at this time as the data also forms part of an ongoing study.

References

[1] B.L. Mordike, Creep-resistant magnesium alloys, Mater. Sci. Eng. A. 324 (2002) 103–112. https://doi.org/10.1016/S0921-5093(01)01290-4.

[2] H. Beladi, M.R. Barnett, Influence of aging pre-treatment on the compressive deformation of WE54 alloy, Mater. Sci. Eng. A. 452–453 (2007) 306–312. https://doi.org/10.1016/j.msea.2006.10.125.

[3] J.A. Yasi, L.G. Hector, D.R. Trinkle, First-principles data for solid-solution strengthening of magnesium: From geometry and chemistry to properties, Acta Mater. 58 (2010) 5704–5713. https://doi.org/10.1016/j.actamat.2010.06.045.

[4] N. Mo, I. McCarroll, Q. Tan, A. Ceguerra, J. Cairney, H. Dieringa, Y. Huang, B. Jiang, F. Pan, M. Bermingham, M.-X. Zhang, Roles of Nd and Mn in a new creep-resistant magnesium alloy, Mater. Sci. Eng. A. 779 (2020) 139152. https://doi.org/10.1016/j.msea.2020.139152.

[5] S. Lv, F. Meng, X. Lu, Q. Yang, X. Qiu, Q. Duan, J. Meng, Influence of Nd addition on microstructures and mechanical properties of a hot-extruded Mg−6.0Zn−0.5Zr (wt.%) alloy, J. Alloys Compd. 806 (2019) 1166–1179. https://doi.org/10.1016/j.jallcom.2019.07.300.

[6] L. Gao, R.S. Chen, E.H. Han, Solid solution strengthening behaviors in binary Mg–Y single phase alloys, J. Alloys Compd. 472 (2009) 234–240. https://doi.org/10.1016/j.jallcom.2008.04.049.

[7] L. Gao, R.S. Chen, E.H. Han, Effects of rare-earth elements Gd and Y on the

solid solution strengthening of Mg alloys, J. Alloys Compd. 481 (2009) 379–384. https://doi.org/10.1016/j.jallcom.2009.02.131.

[8] Q. Peng, X. Hou, L. Wang, Y. Wu, Z. Cao, L. Wang, Microstructure and mechanical properties of high performance Mg–Gd based alloys, Mater. Des. 30 (2009) 292–296. https://doi.org/10.1016/j.matdes.2008.04.069.

[9] S.K. Das, Y.-B. Kang, T. Ha, I.-H. Jung, Thermodynamic modeling and diffusion kinetic experiments of binary Mg–Gd and Mg–Y systems, Acta Mater. 71 (2014) 164–175. https://doi.org/10.1016/j.actamat.2014.02.029.

[10] Z. Huang, C. Yang, L. Qi, J.E. Allison, A. Misra, Dislocation pile-ups at β1 precipitate interfaces in Mg-rare earth (RE) alloys, Mater. Sci. Eng. A. 742 (2019) 278–286. https://doi.org/10.1016/j.msea.2018.10.104.

[11] S.R. Agnew, M.H. Yoo, C.N. Tomé, Application of texture simulation to understanding mechanical behavior of Mg and solid solution alloys containing Li or Y, Acta Mater. 49 (2001) 4277–4289. https://doi.org/10.1016/S1359-6454(01)00297-X.

[12] D. Zhang, H. Wen, M.A. Kumar, F. Chen, L. Zhang, I.J. Beyerlein, J.M. Schoenung, S. Mahajan, E.J. Lavernia, Yield symmetry and reduced strength differential in Mg-2.5Y alloy, Acta Mater. 120 (2016) 75–85. https://doi.org/10.1016/j.actamat.2016.08.037.

[13] L. Wang, Z. Huang, H. Wang, A. Maldar, S. Yi, J.-S. Park, P. Kenesei, E. Lilleodden, X. Zeng, Study of slip activity in a Mg-Y alloy by in situ high energy X-ray diffraction microscopy and elastic viscoplastic self-consistent modeling, Acta Mater. 155 (2018) 138–152. https://doi.org/10.1016/j.actamat.2018.05.065.

[14] R.B. Figueiredo, T.G. Langdon, Achieving superplastic properties in a ZK10 magnesium alloy processed by equal-channel angular pressing, J. Mater. Res. Technol. 6 (2017) 129–135. https://doi.org/10.1016/j.jmrt.2016.05.005.

[15] M. Álvarez-Leal, A. Orozco-Caballero, F. Carreño, O.A. Ruano, Superplasticity in a commercially extruded ZK30 magnesium alloy, Mater. Sci. Eng. A. 710 (2018) 240–244. https://doi.org/10.1016/j.msea.2017.10.093.

[16] T. Vávra, P. Minárik, J. Veselý, R. Král, Excellent superplastic properties achieved in Mg–4Y–3RE alloy in high strain rate regime, Mater. Sci. Eng. A. 784 (2020). https://doi.org/10.1016/j.msea.2020.139314.

[17] E.M. Taleff, P.J. Nevland, P.E. Krajewski, Tensile ductility of several commercial aluminum alloys at elevated temperatures, Metall. Mater. Trans. A. 32 (2001) 1119–1130. https://doi.org/10.1007/s11661-001-0123-9.

[18] T.R. McNelley, K. Oh-Ishi, A.P. Zhilyaev, S. Swaminathan, P.E. Krajewski,

E.M. Taleff, Characteristics of the Transition from Grain-Boundary Sliding to Solute Drag Creep in Superplastic AA5083, Metall. Mater. Trans. A. 39 (2008) 50–64. https://doi.org/10.1007/s11661-007-9401-5.

[19] W.R. Cannon, O.D. Sherby, High temperature creep behavior of Class I and Class II solid solution alloys, Met. Trans. 1 pp. 1030–1032 (1970). http://inis.iaea.org/Search/search.aspx?orig_q=RN:1002326 (accessed June 2, 2020).

[20] M.S. Soliman, F.A. Mohamed, Creep transitions in an Al-Zn alloy, Metall. Trans. A. 15 (1984) 1893–1904. https://doi.org/10.1007/BF02664903.

[21] O.D. Sherby, E.M. Taleff, Influence of grain size, solute atoms and second-phase particles on creep behavior of polycrystalline solids, Mater. Sci. Eng. A. 322 (2002) 89–99. https://doi.org/10.1016/S0921-5093(01)01121-2.

[22] D.A. Woodford, Strain-Rate sensitivity as a measure of ductility, ASM AmerSoc Met. Trans Quart 62 291-3Mar 1969. (1969). https://www.osti.gov/servlets/purl/4799176.

[23] T.G. Langdon, The mechanical properties of superplastic materials, Metall. Trans. A. 13 (1982) 689–701. https://doi.org/10.1007/BF02642383.

[24] J.F. Nie, B.C. Muddle, Characterisation of strengthening precipitate phases in a Mg–Y–Nd alloy, Acta Mater. 48 (2000) 1691–1703. https://doi.org/10.1016/S1359-6454(00)00013-6.

[25] O.A. Ruano, J. Wadsworth, O.D. Sherby, Deformation mechanisms in an austenitic stainless steel (25Cr-20Ni) at elevated temperature, J. Mater. Sci. 20 (1985) 3735–3744. https://doi.org/10.1007/BF01113782.

[26] O.D. Sherby, M. Carsí, W.J. Kim, D.R. Lesueur, O.A. Ruano, C.K. Syn, E.M. Taleff, J. Wadsworth, Mechanical Property - Microstructure Relations in Iron-Carbon Alloys from 1.0 to 5.2% Carbon, in: THERMEC'2003, Trans Tech Publications Ltd, 2003: pp. 11–18. https://doi.org/10.4028/www.scientific.net/MSF.426-432.11.

[27] A.J. Carpenter, A.J. Barnes, E.M. Taleff, High-Temperature Deformation of Magnesium ElektronTM 43, in: Superplast. Adv. Mater. - ICSAM 2012, Trans Tech Publications Ltd, 2013: pp. 93–100. https://doi.org/10.4028/www.scientific.net/MSF.735.93.

[28] O.A. Ruano, F. Carreño, M. Carsí, Ductility and Stability in Metallic Materials, in: THERMEC 2018, Trans Tech Publications Ltd, 2019: pp. 2319–2324. https://doi.org/10.4028/www.scientific.net/MSF.941.2319.

[29] M.T.P. Prado, C.M. Cepeda-Jiménez, Strength ceiling smashed for light metals, Nature. 528 (2015) 486–487. https://doi.org/10.1038/528486a.

[30] C.M. Cepeda-Jiménez, M. Castillo-Rodríguez, M.T. Pérez-Prado, Origin of the low precipitation hardening in magnesium alloys, Acta Mater. 165 (2019) 164–176. https://doi.org/10.1016/j.actamat.2018.11.044.

[31] C.Y. Wang, C.M. Cepeda-Jiménez, M.T. Pérez-Prado, Dislocation-particle interactions in magnesium alloys, Acta Mater. (2020). https://doi.org/10.1016/j.actamat.2020.04.055.

[32] D.F. Shi, M.T. Pérez-Prado, C.M. Cepeda-Jiménez, Effect of solutes on strength and ductility of Mg alloys, Acta Mater. 180 (2019) 218–230. https://doi.org/10.1016/j.actamat.2019.09.018.

[33] T.R. McNelley, D.J. Michel, A. Salama, The Mg-concentration dependence of the strength of A1-Mg alloys during glide-controlled deformation, Scr. Metall. 23 (1989) 1657–1662. https://doi.org/10.1016/0036-9748(89)90338-4.

[34] M.R. Barnett, A taylormodel based description of the proof stress of magnesium AZ31 during hot working, Metall. Mater. Trans. A. 34 (2003) 1799–1806. https://doi.org/10.1007/s11661-003-0146-5.